JCI insight

CD3-downregulation identifies T-helper-cells with superior functionality and distinct metabolism in SARS-CoV2-vaccination- and recall-antigen-specific immunity

Arne Sattler, … , Christian Conrad, Katja Kotsch

JCI Insight. 2024. https://doi.org/10.1172/jci.insight.166833.

Research In-Press Preview Immunology Vaccines

Graphical abstract

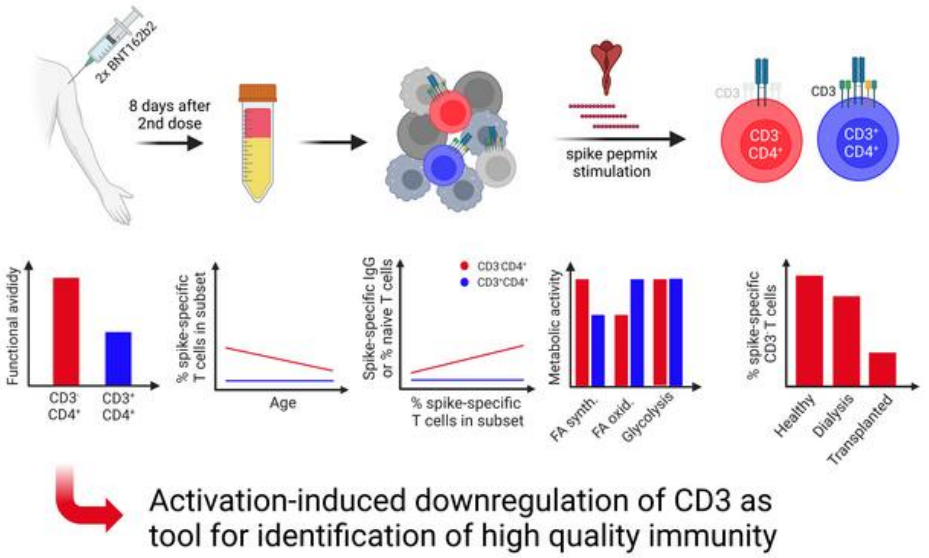

Find the latest version:

https://jci.me/166833/pdf

CD3-downregulation identifies T-helper-cells with superior functionality and distinct metabolism in SARS-CoV2-vaccination- and recall-antigen-specific immunity

Arne Sattler[1], Stefanie Gamradt[2,3], Vanessa Proß[1], Linda Marie Laura Thole[1], An He[1], Eva Vanessa Schrezenmeier[4], Katharina Jechow[5], Stefan M. Gold[2,3,6], Sören Lukassen[5], Christian Conrad[5] and Katja Kotsch[1]

[1]Charité–Universitätsmedizin Berlin, corporate member of Freie Universität Berlin, Humboldt-Universität zu Berlin, and Berlin Institute of Health; Department for General and Visceral Surgery, Berlin, Germany

[2]Charité–Universitätsmedizin Berlin, corporate member of Freie Universität Berlin, Humboldt-Universität zu Berlin, and Berlin Institute of Health; Klinik f. Psychiatrie u. Psychotherapie – Campus Benjamin Franklin, Germany

[3]Charité–Universitätsmedizin Berlin, corporate member of Freie Universität Berlin, Humboldt-Universität zu Berlin, and Berlin Institute of Health; Med. Klinik m.S. Psychosomatik – Campus Benjamin Franklin, Berlin, Germany

[4]Charité–Universitätsmedizin Berlin, corporate member of Freie Universität Berlin, Humboldt-Universität zu Berlin, and Berlin Institute of Health; Department of Nephrology and Intensive Care, Berlin, Germany

[5]Charité–Universitätsmedizin Berlin, corporate member of Freie Universität Berlin, Humboldt-Universität zu Berlin, and Berlin Institute of Health; Center for Digital Health, Berlin, Germany

[6]Universitätsklinikum Hamburg Eppendorf, Institut für Neuroimmunologie und Multiple Sklerose (INIMS), Zentrum für Molekulare Neurobiologie, Hamburg, Germany

Corresponding Authors:

Arne Sattler, Charité-Universitätsmedizin Berlin, Department for General and Visceral Surgery, Hindenburgdamm 30, 12203 Berlin, Germany, arne.sattler@charite.de, +49 30 450552427

Katja Kotsch, Charité-Universitätsmedizin Berlin, Department for General and Visceral Surgery, Hindenburgdamm 30, 12203 Berlin, Germany, katja.kotsch@charite.de, +49 30 450652247

Conflict-of-interest:

KK received unconditional funding from Chiesi GmbH (Germany). SG received personal fees from Abcam (Germany) for a webinar presentation. The funders were not involved in the study design, collection, analysis, interpretation of data, the writing of this article or the decision to submit it for publication. All other authors have declared that no conflict of interest exists.

Abstract

Functional avidity is supposed to critically shape the quality of immune responses, thereby impacting host protection against infectious agents including SARS-CoV2. Here we show that after human SARS-CoV2 vaccination, a large portion of high-avidity spike-specific $CD4^+$ T cells lose CD3 expression after *in vitro* activation. The $CD3^-$ subset is enriched for cytokine positive cells, including elevated per-cell expression levels, and shows increased polyfunctionality. Assessment of key metabolic pathways by flow cytometry revealed that superior functionality is accompanied by a shift towards fatty acid-synthesis at the expense of their oxidation, whereas glucose transport and glycolysis were similarly regulated in SARS-CoV2-specific $CD3^-$ and $CD3^+$ subsets. As opposed to their $CD3^+$ counterparts, frequencies of vaccine-specific $CD3^-$ T cells positively correlate with both the size of the naïve $CD4^+$ T cell pool and vaccine-specific IgG levels. Moreover, their frequencies negatively correlate with advancing age and are impaired in patients under immunosuppressive therapy. Typical recall-antigen-reactive T cells show a comparable segregation into functionally and metabolically distinct $CD3^+$ and $CD3^-$ subsets, but are quantitatively maintained upon ageing, likely due to earlier recruitment in life. In summary, our data identify $CD3^-$ T helper cells as correlates of high quality immune responses that are impaired in at-risk populations.

Brief Summary:

Activation-induced loss of CD3 marks high-avidity, multipotent SARS-Cov2-vaccine- and recall-antigen-specific T cells with distinct metabolism that are reduced in the elderly and individuals with comorbidities.

Introduction

The quality of immune responses is considered to critically determine outcomes after infection, vaccination or in context with anti-tumor immunity. However, only few tools allow assessment of parameters that unequivocally reflect functional superiority of molecular or cellular immune features in humans. Among those, quantification of neutralizing antibody levels is key to estimate antiviral protection e.g. against SARS-CoV2 (1) or influenza virus (2). Long-term non-progression after Human immunodeficiency virus (HIV) infection has been found to correlate with increased quantities of polyfunctional T cells (3, 4) that are also characteristically enriched in individuals experiencing mild vs. severe SARS-CoV2 infections (5). Vice versa, immunophenotyping of COVID-19 patients suggested that preconditions such as higher comorbidity index or advanced age are associated with reduced frequencies of virus-reactive interferon gamma (IFNγ) secreting T helper cells in infected individuals (6), contributing undesirable COVID19- prognosis. The concept of altered T cell function in severe disease was further substantiated by Bacher et al., showing that SARS-CoV2-specific, *in vitro* generated short-term T cell lines of non-hospitalized patients respond to lower antigen concentrations than those from severe cases (7), indicating higher functional avidity.

The limitations of such labor and time-intensive approach for large-scale individual evaluation have been recently overcome by data from Loyal et al., revealing that $CD4^+$ T cells with reduced surface CD3 expression show increased functional avidity in SARS-CoV2 infected individuals (8). Although loss of T cell receptor- (9) or CD3-expression in response to T cell stimulation has been described earlier for both $CD4^+$ (10) and $CD8^+$ subsets (11), CD3 dim or negative T cells have been excluded from studies comprehensively assessing vaccine-specific immunity so far. We therefore set out to compare classical $CD3^+CD4^+$ T helper cell responses with those of their $CD3^-$ counterparts in healthy individuals after standard SARS-CoV2 mRNA vaccination and in response to viral recall antigens. Our analyses demonstrate that vaccine-specific $CD3^-$ Th cells are superior with respect to their functional avidity, show distinct metabolic programming, and their reduced mobilization into novel vaccine-induced immune

responses is characteristic for an ageing immune system. In summary, our data suggest that identification of high avidity T helper cells based on activation-induced downregulation of CD3 could serve as an important tool for risk assessment of vulnerable patient groups in the context of vaccination or infection and might facilitate selection of superior clones for therapeutical purposes such as adoptive T cell transfer.

Results

Segregation of SARS-CoV2 spike protein-specific $CD4^+$ T cells into $CD3^+$ and $CD3^-$ subsets after mRNA vaccination

For detection of SARS-CoV2 spike-specific $CD4^+$ T helper cells, PBMC were obtained 8±1 days after the second dose of a 2-dose standard mRNA vaccination (BioNTech/Pfizer) of virus-naïve individuals and stimulated with an overlapping peptide pool encompassing the complete viral spike protein. After gating on $dump^{negative}$ live lymphocytes, specific cells were assessed both within the $CD3^+$ and $CD3^-$ compartment. Interestingly, pre-gating on $CD3^-$ T cells revealed a small CD4 positive to dim subset enriched for specific $CD154^+CD137^+$ T cells (Fig. 1A). Overall, spike-specific T cells were identified in all but one donor in both compartments (Fig. 1B, left). Relative frequencies within the $CD3^-CD4^+$ subset were significantly enriched around tenfold (mean: 17.92 % +/- 2.120) as compared to the $CD3^+CD4^+$ fraction (mean: 0.1759 % +/- 0.01807) (Fig. 1B, middle). Cell counts within both subpopulations did not exhibit significant differences but tended to be moderately lower within the $CD3^-CD4^+$ compartment (Fig. 1B, right) that was further characterized by significantly reduced CD4 expression (Fig. 1C) as reflected by lower mean fluorescence intensity (MFI) levels. Quantification of spike-specific $CD3^+CD4^+$ and $CD3^-CD4^+$ T cells with four different, commercially available anti-CD3 clones conjugated to the same fluorochrome (Supplemental Figure 1A) yielded comparable results (Supplemental figure 1B). Both subsets were largely $CD28^+$ and did not show expression of the NK cell associated molecules CD16, CD56 and CD94 (Supplemental Figure 2), suggesting that they are bona fide T cells. To address whether these vaccine-specific T cells lacked CD3 expression ex vivo or downregulated the molecule in a stimulation-dependent manner, PBMC were stained and analyzed as before with the exception that CD3 was labeled either before or after stimulation. In pre-experiments, we determined CD3 pre-staining to be stable over the culture period with some acceptable loss of fluorescence intensity (Supplemental Figure 3A, upper left vs. lower left plot). Of note, only few spike-specific T cells were detectable within $CD3^-$ T cells when samples were stained prior to stimulation. In contrast, more than 15-fold

higher frequencies of antigen-reactive $CD154^+CD137^+$ T cells were identified when samples were labeled after stimulation (Supplemental Figure 3A and B), indicating that CD3 is largely downregulated as a consequence of stimulation in a subset of specific T cells. To substantiate this notion, spike-specific $CD3^-CD4^+CD154^+CD137^+$ were MACS-pre-enriched, followed by FACS purification (Supplemental Figure 3C) and expanded for 10 days in vitro with cytokines and autologous feeder cells in the absence of antigen. CD3 (re-) expression levels in $CD3^-CD4^+$ and $CD3^+CD4^+$ -derived T cell lines were comparable after the expansion period (Figure 1D). Upon antigen-specific restimulation, $CD3^-CD4^+$ derived lines downregulated CD3 again in an antigen concentration-dependent manner as reflected by decreasing mean fluorescence intensity levels (Figure 1E). We next assessed whether the spike-specific $CD3^-CD4^+$ population could also be detected after single peptide stimulation. Several reports (8, 12, 13) suggested that a 15-mer encompassing amino acids (aa) 816-830 is recognized by 20-60 % of healthy probands and up to 100 % in individuals expressing the MHC class II allele DPA1*01:03 (8). We therefore stimulated PBMC of a vaccinated, $DPA1*01:03^+$ heterozygous blood donor with full spike peptide mix vs. aa816-830 peptide. As already demonstrated, full spike stimulation yielded similar counts of specific cells in both compartments, associated with an enrichment of $IFN\gamma^+$ cells in the $CD3^-CD4^+$ subset. After aa816-830 stimulation, specific cells were detectable in both compartments with a quantitative dominance of $CD3^+CD4^+$ over $CD3^-CD4^+$ T cells. Vice versa, frequencies of IFNγ producers were elevated in the $CD3^-CD4^+$ subpopulation (Supplemental Figure 4).

Correlation of spike-reactive $CD3^-CD4^+$ T cells with specific IgG levels, age and the size of the naïve T cell pool

We detected a moderate positive correlation between specific T cell frequencies in both subsets (Fig. 2A). Over 7 decades of life, relative portions of vaccine-specific $CD3^-CD4^+$ T cells slightly, but significantly decreased, whereas frequencies of their $CD3^+$ counterparts remained constant (Fig. 2B). Importantly, only frequencies of spike-specific $CD3^-CD4^+$ T cells, but not of

$CD3^+CD4^+$ positively correlated with spike S1 specific IgG levels (Fig. 2C). Furthermore, frequencies of the $CD3^-CD4^+$ fraction were strongly associated with increased portions of bulk naïve $CD3^+CD4^+CD45RA^+CD62L^+$ T cells (Fig. 2D; with the gating strategy depicted in Supplemental Figure 5A). Advanced age was strongly associated with both reduced antibody levels (Fig. 2E) as well as frequencies of bulk naïve T cells (Fig. 2F). In a limited number of individuals, we analyzed frequencies of specific T cells at different time points (range: 19-262 days, mean: 98.65 days) post vaccination in a cross-sectional manner. Specific $CD3^+CD4^+$ and $CD3^-CD4^+$ subsets were detectable in all samples and remained comparably stable over the observation period with no significant decline in frequencies (Supplemental Figure 6). Vaccine-specific $CD3^-CD4^+$ T cells showed slightly, but significantly higher frequencies of $CD45RO^+CD62L^-$ effector/memory-type T cells (Fig. 2G, gating strategy in Supplemental Figure 5A); interestingly they were characterized by reduced portions of proliferating $Ki67^+$ cells (Fig. 2H, left, with gating strategy in Supplemental Figure 5A), being in line with diminished percentages of recently in vivo activated $PD1^+$ cells (Fig. 2H, right with gating strategy in Supplemental Figure 5A). Females showed higher frequencies of spike-specific $CD3^-CD4^+$, but not $CD3^+CD4^+$T cells than males (Supplemental Figure 7A); both groups were characterized by a comparable age composition (Table I).

In summary, $CD3^-CD4^+$ frequencies associate with vaccine-specific titers, are diminished with increasing age and their quantitative recruitment into SARS-CoV2-specific vaccine responses is augmented in individuals harboring elevated portions of naïve T cells.

Distinct metabolic features characterize vaccine-specific $CD3^-CD4^+$ T cells

Recent reports have defined key metabolic proteins, including rate-limiting enzymes, for robust single cell assessment of the metabolic state by flow or mass cytometry, using validated antibodies (14, 15). For pioneering quantification of multimodal metabolic features within rare antigen-specific T cells, we designed a FACS panel characterizing components critical for glucose uptake (glucose transporter 1, GLUT1), glycolysis (hexokinase 2, HK2), tricarboxylic

acid cycle (isocitrate dehydrogenase 2, IDH2), oxidative pentose phosphate pathway (Glucose-6-phosphate dehydrogenase, G6PD), ATP synthesis (ATP synthase subunit alpha, ATP5A), lactate metabolism/aerobic glycolysis (lactate dehydrogenase, LDH), fatty acid synthesis (acetyl-CoA carboxylase alpha, ACAC) and -oxidation (carnitine palmitoyl-transferase 1A, CPT1A). An overview of the covered metabolic pathways is depicted in Figure 3A. To assess immune metabolism in specific T cells, PBMC were stimulated and spike-reactive $CD154^{+}CD137^{+}$ $CD3^{+}$ and $CD3^{-}$ Th cell subsets identified as before, along with expression analysis of metabolic markers based on their individual mean fluorescence intensity (MFI). In all analyses, the non-reactive $CD3^{+}CD4^{+}CD154^{-}CD137^{-}$ T cell population (termed “bulk” in the respective figures) served as internal control. Overall, specific $CD3^{+}$ and $CD3^{-}$ T-cell subsets similarly employed glycolysis after activation, as mirrored by comparable upregulation of GLUT1 and HK2 over controls; the same applied to expression levels of LDH, a critical enzyme during aerobic glycolysis which is a hallmark of metabolic reprogramming in activated T cells. Interestingly, ATP synthesis as reflected by ATP5a expression was substantially downregulated in both subsets as compared to non-reactive controls. Importantly, the fatty acid synthesis pathway represented by ACAC expression was significantly upregulated in $CD3^{-}$ over $CD3^{+}$ T cells and controls. Concomitantly, specific $CD3^{-}$ but not $CD3^{+}$ Th cells reduced fatty acid oxidation, given their significantly lower expression levels of CPT1A. Spike-specific $CD3^{-}$ Th cells were further characterized by reduced activation-dependent downregulation of IDH2 over their $CD3^{+}$ counterparts and a moderate increase of G6PD expression over both $CD3^{+}$ and control Th cells (Figure 3B).

As a conclusion, Spike-specific $CD3^{-}CD4^{+}$ T cells stand out with respect to their augmented metabolic switch to fatty acid synthesis, being associated with significant downregulation of fatty acid oxidation as compared to $CD3^{+}CD4^{+}$ and control Th cells.

$CD3^-CD4^+$ are functionally superior to their $CD3^+$ counterparts

To assess the functional potential of spike-specific $CD3^-CD4^+$ vs. $CD3^+CD4^+$ T cells, cytokine production was both analyzed on the population level and per cell with the gating strategy depicted in Supplemental Figure 5B. The $CD3^-CD4^+$ subset contained significantly higher frequencies of $IFN\gamma^+$, $IL\text{-}2^+$, $IL\text{-}4^+$, but not $TNF\alpha^+$ cells (Fig. 4A and B). This difference also applied to the amount of IFNγ (Fig. 4A, right) and IL-4 (Supplemental Figure 7B, right) expressed per cell as evidenced by higher mean fluorescence intensity levels and to frequencies of $IFN\gamma^+TNF\alpha^+IL\text{-}2^+$ co-producing polyfunctional T cells (Fig. 4C and D). Interestingly, MFI levels of the growth factor IL-2 were significantly reduced in the $CD3^-$ subset (Supplemental Fig. 7B, middle). To validate data that functional superiority relies on higher functional avidity (8), PBMC were stimulated with spike peptide mix; $CD154^+$ cells were pre-enriched by MACS, followed by FACS-purification of specific $CD3^-CD4^+$ and $CD3^+CD4^+$ subpopulations (Supplemental Figure 3C) and in vitro expansion. After specific restimulation with titrated amounts of antigen, the $CD3^-CD4^+$ subset contained substantially higher frequencies of cells producing IFNγ, IL-2 or IL-4 than their $CD3^+$ counterparts regardless of what antigen concentration was used: the $CD3^-CD4^+$ population still produced cytokines at low antigen concentrations at which the $CD3^+CD4^+$ population was already cytokine-negative (Figure 4E).

Quantitative, functional and metabolic features of typical recall-antigen-specific $CD3^-CD4^+$ T cells

We next addressed whether separation into $CD3^-CD4^+$ and $CD3^+CD4^+$ T cell subsets could not only be detected in de-novo vaccinated, previously virus-naive individuals, but also accounts for typical recall-antigen-specific responses. Therefore, analyses were conducted as before for T helper cells reactive to a peptide mix consisting of CMV, EBV- and influenza antigens, termed CEF that were detectable in all individuals (Fig. 5A, left). In analogy to their spike-specific counterparts, CEF-specific T cells also segregated into $CD3^+CD4^+$ and $CD3^-$

$CD4^+$ subsets with the latter bearing significantly higher frequencies (mean: 0.07 % +/- 0.01385 vs. 13.39 % +/- 1.794) (Fig. 5A, middle), showing significantly higher counts (Fig. 5A, right) and a strong downregulation of CD4 (Fig. 5B). In addition, frequencies of both subpopulations showed a highly significant positive correlation (Fig. 5C). Of note, as opposed to our findings for spike-specific T cells, portions of $CD3^-CD4^+$ CEF specific T cells did not diminish with age, whereas frequencies of the $CD3^+CD4^+$ subset increased slightly, but significantly with advanced age (Figure 5D). Both subsets showed a negative correlation with frequencies of naïve T cells; however, this observation reached significance only for the $CD3^+CD4^+$ population (Fig. 5E).

Significantly elevated frequencies of cytokine-positive cells were also detected within CEF reactive $CD3^-CD4^+$ as compared to $CD3^+CD4^+$ T cells; this observation most pronounced for IFNγ, applied to TNFα and IL-2, but excluded IL-4 or polyfunctionality (Fig. 6A-C). Significantly higher per-cell expression levels within the $CD3^-CD4^+$ compartment was only noted for IFNγ (Fig. 6A, right), whereas a slight decrease was observed for IL-2 (Supplemental Fig. 7C).

Interestingly, CEF-specific Th cells revealed similar metabolic features as already determined for the spike-specific population. Thus, fatty acid synthesis as reflected by ACAC expression levels was particularly upregulated in the CEF-specific CD3-$CD4^+$ subset, along with significantly diminished fatty acid oxidation mirrored by reduced CPT1a expression and reduced downregulation of G6PD as compared to the $CD3^+CD4^+$ subset. Although HKII-levels were only slightly upregulated in both CEF-subpopulations over controls, significantly elevated expression of GLUT1 over controls is suggestive of increased glucose metabolism (Figure 6D).

Quantitative and functional impairment of spike-specific $CD3^-CD4^+$ T cells in patients under immunosuppressive therapy

Patients with comorbidities, including those under dialysis or after solid organ transplantation, are prone to experience more severe COVID-19 disease courses (16, 17) and show multiple

impairments in humoral and cellular SARS-CoV2 vaccine-specific immunity (18, 19). We therefore examined vaccination-induced $CD3^{-}CD4^{+}$ T cells in patients with renal insufficiency on dialysis and kidney transplant recipients under standard immunosuppressive therapy. Both groups were age-matched with healthy probands (Table II); all samples were consistently examined 8±1 days after the second standard mRNA vaccination. Interestingly, being in line with previous reports on conventional T helper cell responses (18, 20, 21), dialysis patients were characterized by only moderate reduction of spike-specific $CD3^{-}CD4^{+}$ T cells (mean: 12.36 % +/- 2.671) in comparison to controls (17.31 % +/- 3.202). However, transplant recipients showed a significant reduction of $CD3^{-}CD4^{+}$ T cell frequencies (mean: 5.871 % +/- 1.513) compared to healthy probands (Figure 7A) and a significant expansion of specific $CD3^{+}CD4^{+}$ counts at the expense of the $CD3^{-}CD4^{+}$ population (Fig. 7B). Of note, the $CD3^{-}$ subset in transplant recipients did not exhibit characteristics of superior cytokine production (Fig. 7C) that were observed in healthy individuals (Fig. 4A-D). In summary, spike-specific $CD3^{-}CD4^{+}$ T cells transplant recipients under immunosuppressive medication are numerically and functionally devoid of typical hallmarks found in healthy probands.

Discussion

Definition and straightforward analysis of key parameters reflecting the quality of vaccine-specific immunity are of particular interest for predicting disease outcomes in at-risk groups. Here we used differential CD3 expression on human Th cells as an easily applicable tool that may explain fundamental aspects of unsatisfactory immune responses after vaccination in the elderly and patients with preconditions. At the same time, it could be used as a new biomarker for general assessment of high-quality immune responses. Our data on SARS-CoV2 mRNA vaccine-specific T helper cells build on the recent finding of a novel $CD4^+$ subpopulation that rapidly downregulates CD3 expression in response to in vitro stimulation in SARS-CoV2 infected individuals (8). After SARS-CoV2 mRNA vaccination, we found this population to be of comparable size as its "classical" $CD3^+$ counterpart being reflected by similar total counts. With respect to typical viral recall antigen-specific responses, the CEF-specific $CD3^-$ subset even outnumbered conventional $CD3^+$ Th cells by a factor of 2, highlighting that a substantial fraction of the specific T helper cell pool had been excluded in commonly employed FACS-dependent stimulation assays so far. Based on our data, inclusion of the $CD3^-$ subset for studying vaccine-specific cellular immunity seems of prime importance given their superior functional avidity as reflected by a lower activation threshold and increased cytokine secretion and polyfunctionality on a population- and per-cell level. Key characteristics of vaccine-reactive $CD3^-$ T cells further encompass distinct regulation of fatty acid metabolism, their positive correlation with the size of the naïve T cell pool and an age-dependent decline that was not observed for conventional $CD3^+$ Th cells.

With the advent of SARS-CoV2, comprehensive analysis of antiviral immunity in large patient cohorts provided new insights into how cellular immunity measures might correlate with disease outcomes. So far, however, only few studies exist that bridge individual pre-disposing factors with immune measures beyond antibody levels that are distinctly regulated in at-risk groups, leading to undesired outcomes after infection or vaccination. In that respect, we previously showed that advanced age or increased comorbidity index shape the specific Th

cell response towards reduced interferon gamma production in SARS-CoV2-infected patients (6), a feature that was recapitulated in aged SARS-CoV2 mRNA vaccinees (22). In the light of our novel data and in concert with findings on impaired functional avidity of T helper cell responses in severe COVID-19 (7), the aforementioned functional limitations are likely resulting from reduced recruitment of high-avidity T cells with superior cytokine production capacity. Whereas a relation between advanced age and reduced thymic output (leading to up to 50% loss of naïve T cell counts in individuals aged >60 years as compared to adolescents) is long-anticipated to impair immunocompetence in the elderly (23), our study suggests that it is particularly high-avidity responses that are quantitatively compromised, resulting from an increasingly limited naïve T cell pool. In support of this finding, bulk naïve T cell counts pre-vaccination proved to be the best predictor for protective titers after A(H1N1)pdm09 influenza vaccination with both measures being diminished with advancing age (24).

Our comprehensive characterization of specific $CD3^-$ T cell biology included assessment of cell metabolism. Focusing on validated antibodies detecting key protein targets, mostly rate-limiting enzymes (14, 15, 25), this innovative cytometry-based approach allows a sensitive quantification of metabolic activity with single cell resolution, thereby enabling us to apply this technology to the analysis of rare antigen-specific T cells. In general, protein-based analyses might more accurately reflect a cells' metabolic state than transcriptome-based studies, given that regulation of metabolic pathways has been shown to dominantly occur on the translational rather than transcriptional level (26). As a key finding, our data highlight significant differences in fatty acid metabolism between antigen-specific $CD3^-$ and $CD3^+$ subsets. The fact that ACAC expression was highest in the $CD3^-$ subset suggests increased fatty acid demand being characteristic for this subset upon activation, along with reduced fatty acid oxidation via CPT1a, possibly resulting from its blockade by ACAC-synthesis product malonyl-CoA (27). Of note, mice with T cell specific ACAC deletion fail to generate efficient Th1 responses, produce less IFNγ and succumb early to M. tuberculosis infection (28). Together with the finding that ACAC deletion or blockade reduces Th1-mediated inflammation in experimental colitis (29) and limits excessive IFNγ production in human autoimmunity (30), these aspects contextualize the

increased demand for fatty acid synthesis with superior execution of effector functions, including IFNγ production, in Spike- and CEF-specific $CD3^-$ T cells.

Our findings on increased GLUT1, HK2 and LDH expression in both T cell subsets confirm several other studies on bulk T cells demonstrating augmented aerobic glycolysis (also known as Warburg effect) upon polyclonal activation (31, 32). At the same time, as opposed to the bulk analyses performed by Ahl at al. using αCD3/CD28 stimulation (14), our results highlight that not all metabolic pathways are comparably upregulated upon antigen-specific (i.e. physiologic) TCR triggering. This applied to IDH2 and ATP5a, showing reduced expression over unstimulated controls in spike-activated T cells, which is concomitant with the well-described switch from oxidative metabolism to aerobic glycolysis to support rapid effector function after activation (33, 34).

Of note, metabolic protein expression patterns similarly applied to spike- and CEF-specific responses, arguing for common metabolic requirements in established memory/effector-type Th cells regardless of their specificity.

As another common motif for spike- and CEF-specific responses, we found $CD3^-CD4^+$ T cells to express less IL-2 on a per-cell basis. The fact that the quantity of autocrine IL-2 could directly impact specific T cell expansion (35) might explain why we detected slightly, but significantly reduced frequencies of proliferating and in vivo activated $PD1^+$ T cells within this subset. Interestingly, this aspect seems counterintuitive, based on the assumption that high-avidity T cells exhibit superior proliferation capacity. However, this phenomenon might be explained by the comparably high antigen dose and sustained local protein availability associated with mRNA vaccination (36, 37). In that context, the functional potential of high avidity cytotoxic T cells was demonstrated to be critically linked to antigen dose with supraoptimal concentrations limiting cellular expansion in vivo and in vitro (38).

As a side aspect, we could also detect specific T cells in a blood donor with an MHC class II background predicted to respond to a single spike derived 15-mer. At first glance, it might surprise that we identified reactive cells both in the $CD3^-CD4^+$ and $CD3^+CD4^+$ compartment. It

needs to be considered, however, that a given peptide might induce polyclonal responses as has been demonstrated for influenza (39), resulting in clonotypes with different functional avidity, that may or may not downregulate CD3 upon stimulation.

Focusing on patients with preconditions, we found individuals under immunosuppressive therapy, but not under hemodialysis, to harbor significantly reduced frequencies of specific $CD3^-$ T cells as compared to age-matched controls. It is tempting to speculate whether this phenomenon could be simply explained by direct therapy-dependent suppression of vaccine-specific T cell activation, expansion and memory differentiation or might involve a recently described mechanism where recurring herpesvirus infections, being common in immunosuppressed individuals (40), lead to contraction of the naïve T cell pool in aged individuals, thereby limiting vaccination success (41).

Another important aspect of our study is the fact that only frequencies of $CD3^-$, but not of conventional $CD3^+$ T cells correlate with SARS-CoV2-S1 domain specific antibody titers, suggesting a more productive interaction of the latter with B cells. It needs to be determined whether this involves augmented cytokine or relies on other features regulating lymph node crosstalk during priming and/or memory formation.

Limitations of the data presented herein include the absence of an individual follow-up of spike-specific $CD3^-$ T cells over time that is hampered by different SARS-CoV2 infection and re-vaccination fates within our cohort; we were only able to provide information on spike-specific T cell stability in a cross-sectional manner. Therefore, it remains to be addressed how the specific $CD3^-$ pool is quantitatively, functionally and metabolically maintained in the absence of antigenic triggers. Our findings on CEF responses suggest that high avidity $CD3^-$ Th cells are kept over decades when recruited early in life, since CMV infection prevalence already reaches up to 36 % in healthy individuals aged 6-11 years (42). It cannot be ruled out, however, that maintenance of high-avidity cells is dependent on recurring viral reactivation and might be critical to maintain functional superiority. In that context, data from animal models indicate that functional avidity might not be static, but could undergo dynamic changes depending on

antigen dose (38). For a comprehensive characterization of high-avidity $CD3^{-}CD4^{+}$ T cells, follow-up studies should include transcriptome and TCR-repertoire analyses, allowing a more profound comparison with their $CD3^{+}CD4^{+}$ counterparts. Finally, although the mechanistic steps leading to downregulation of components of the TCR:CD3 complex have been examined in greater detail, including dynamics of internalization, degradation and prevention of recycling (43-45), the exact physiological relevance of such process beyond limiting excessive inflammation (46) will still be a matter of future investigations. The same holds true for investigation of the exact impact of the $CD3^{-}CD4^{+}$ subset on antiviral protection that needs to be addressed in larger cohorts in a prospective manner.

In summary, our data suggest $CD3^{-}CD4^{+}$ Th cells as correlates of high quality immune responses that may be used for general assessment of immunocompetence in vaccination-, infection- or tumor-related immunity.

Methods

Study design, sex as biological variable, and determination of humoral immunity

Demographics of healthy probands (HC) are depicted in Table I. Information on patients with comorbidities and age matched healthy probands is summarized in Table II. The study examined males and females, and sex-dimorphic effects are reported. All participants were enrolled between January and April 2020 and received a standard two-dose (21 days apart) SARS-CoV2 mRNA vaccine (BioNTech/Pfizer BNT162b2 “Comirnaty”). Blood samples were collected on day 8±1 after the second dose. All individuals were SARS-CoV2-naïve at the time of analysis, provided by frequent point-of-care testing and/or a negative SARS-CoV2 nucleoprotein-specific ELISA (Euroimmun, Lübeck, Germany). Vaccination-induced SARS-CoV2 spike S1 domain-specific IgG levels were analyzed in serum samples at day 8±1 post second dose by ELISA (Euroimmun, Lübeck, Germany). Samples were considered positive with OD ratios of ≥1.1 as per manufacturer´s guidelines. Samples exceeding the upper assay limit (O.D. ratio >10) were pre-diluted and re-measured.

Antigens

Antigen-specific stimulations were conducted with an overlapping peptide mix consisting of 15-mers with 11 amino acids overlap covering the full sequence of the SARS-CoV-2 spike glycoprotein (alpha-variant, “Pepmix”, JPT, Berlin, Germany). In one experiment, a single spike-derived 15-mer encompassing aa816-830 was used (aa-sequence: SFIEDLLFNKVTLAD; JPT). A combination of 15-mer peptide pools including CMV (“Peptivator pp65”, Miltenyi Biotech, Bergisch Gladbach), EBV (“Peptivator consensus”, Miltenyi Biotech) and influenza H1N1 (“Peptivator matrix protein 1”, and “Peptivator nucleoprotein”, Miltenyi Biotech) were used for assessment of recall-antigen-specific responses (termed CEF). Antigens were used at a concentration of 0.5 µg/ml per peptide unless otherwise indicated.

Sample processing and stimulation

Serum was collected and cryopreserved. Peripheral blood mononuclear cells (PBMC) were isolated from heparinized blood by Ficoll-Paque™ density gradient centrifugation and immediately cryopreserved in liquid nitrogen. For analysis of antigen-specific T cells, 3-5x10^6 PMBC per stimulation were thawed, washed twice in pre-warmed RPMI1640 medium (containing 0.3 mg/ml glutamine, 100 U/ml penicillin, 0.1 mg/ml streptomycin, 20% FCS and 25 U/ml Benzonase (Santa Cruz, Dallas, USA)), rested for 2 h in medium (RPMI1640 with glutamine, antibiotics and 10 % human AB serum, all Biochrom, Berlin, Germany) and stimulated with SARS-CoV2 spike or CEF peptide mix for 16 h. Brefeldin A (10 µg/ml, Sigma-Aldrich) was added after 2 h. DMSO was added to the unstimulated controls in the same quantity as in stimulated samples.

Conventional and metabolic flow cytometry

For surface stainings, antibodies against CD3 (SK7, Biolegend, Carlsbad, CA, USA), CD4 (SK3, Becton Dickinson, Franklin Lakes, NJ, USA), CD8 (SK1, Ebioscience, San Diego, CA, USA), CD45RO (UCHL1, BioLegend), CD62L (DREG-56, BioLegend) and PD-1 (EH12.1, Becton Dickinson) were used. In some experiments, anti-CD28 (CD28.2, BioLegend), CD16 (3G8, BD), CD56 (NCAM, BioLegend) and CD94 (DX22, BioLegend) were used.

Undesired cells were excluded via a “dump channel” that contained $CD14^+$ monocytes (M5E2, BioLegend), $CD19^+$ B-cells (HIB19, BioLegend), and dead cells (fixable live/dead, BioLegend). Cells were fixed in FACS Lysing Solution (Becton Dickinson), followed by permeabilization with FACS Perm II Solution (Becton Dickinson). Cells were intracellularly stained with anti-CD154 (24-31, BioLegend), anti-CD137 (4B4-1, BioLegend), anti–TNF-α (MAb11, BioLegend), anti–IFN-γ (4SB3, Ebioscience), anti–IL-2 (MQ1-17H12, BioLegend), anti-Ki67 (B56, Becton Dickinson) and anti-IL-4 (MP4-25D2, BioLegend). Samples were measured on a BD Fortessa X-20 cytometer.

For key metabolic protein detection, representing major metabolic pathways, in antigen-specific T cells, antibodies were chosen that have been described and validated earlier (14, 15), as summarized in Figure 3A. Antibodies (all Abcam) were coupled in-house (CPT1a

(8F6AE9); IDH2 (EPR7577); G6PD (EPR20668); HK (EPR20839); LDH (EP1566Y)) using lightning-link (Abcam) or antibody labelling kits (ThermoFisher) or purchased ready-to-use (GLUT1 (EPR3915); ACAC (EPR4971); ATP5A (EPR13030(B)) and underwent extensive titration in combination with PMT voltration to achieve optimal FACS device sensitivity. PBMC were stimulated and surface stained as described before, followed by fixation and permeabilization with transcription factor staining buffer set (eBioscience, ThermoFisher). All metabolic markers were then stained in perm buffer together with CD154, CD137 and IFNγ; the panel design is depicted in Supplemental Table 1. For metabolic assessment, all samples were measured on a BD Fortessa X-20 cytometer in one batch together with single stain compensation controls, thereby excluding any inter-assay variability.

Generation and restimulation of spike-specific $CD3^+$ and $CD3^-$ $CD4^+$ T cell lines

For generation of short-term antigen-specific T-cell lines, 10^7 PBMC were stimulated for 16 h with spike peptide mix in the presence of anti-CD40 (1 µg/ml, HB14, Miltenyi Biotec) for retention of surface CD154 expression (47). Thereafter, cells were surface stained with anti-CD154 PE (24-31, BioLegend) and magnetically pre-enriched using anti-PE nanobeads (BioLegend) over a MACS LS column (Miltenyi Biotec). Spike-specific $DUMP^-CD154^+CD137^+$ $CD3^-CD4^+$ and $CD3^+CD4^+$ subsets were further sorted to >97 % purity on a FACS Aria Fusion cell sorter (Becton Dickinson). Cells were expanded for 10 days with a 100-fold excess of autologous Mitomycin C (SigmaAldrich)-treated PBMC in the presence of IL-7 and IL-15 (10 ng/ml each, Miltenyi Biotec). Cells were restimulated in the presence of CD3-depleted autologous PBMC (1:5 ratio) for 16 hrs.

FACS data analysis

FACS data was analyzed with FlowJo 10 (Becton Dickinson). The gating strategy for identification of antigen-specific $CD4^+$ T cells is depicted in Figure 1. A T cell response was considered positive when antigen stimulated PBMC contained at least twofold higher frequencies of $CD154^+CD137^+$ $CD4^+$ T cells (stimulation index of 2) as compared to the

unstimulated control with at least twenty events. Co-expression of cytokines was analyzed with the Boolean gating function in FlowJo.

Statistics

Statistical analysis and composition of ELISA and FACS data derived figures were performed using GraphPad Prism 8 (GraphPad, La Jolla, CA, USA). Data distribution was assessed using the Kolmogorov-Smirnov test. Depending on normal distribution or not, ANOVA (with Holm-Sidak´s post-hoc) or Kruskal-Wallis test (with Dunn post-hoc) were chosen for multiple comparisons. For two-group comparisons, t test/Wilcoxon test (depending on data distribution; for paired datasets) or t test/Mann-Whitney test (depending on data distribution; for unpaired datasets) were used. The relationship between two variables was examined by simple linear regression analysis. For analysis of contingency tables, *Fisher's exact* test was applied. In all tests, a value of $p<0.05$ was considered significant.

Study approval

The study protocol was approved by the ethics committee of the Charité-Universitätsmedizin Berlin (EA4/188/20), Universitätsmedizin Greifswald (BB 019/21), and Sachsen-Anhalt (EA7/21) and carried out in compliance with its guidelines. All participants provided written informed consent in accordance with the Declaration of Helsinki.

Data availability

All cellular data needed to evaluate the conclusions in the paper are present in the paper or the Supplementary Materials. Values for all data points in the figures can be found in the Supplemental “Supporting Data Values” Excel file. Requests for materials should be directed to A.S.

Author contributions

AS designed the study, conducted experiments, acquired and analyzed data and wrote the manuscript. SG conducted experiments, acquired and analyzed data and wrote the manuscript. VP, LMLT, AH, EVS and KJ conducted experiments and acquired data. SL analyzed data. SMG, CC and KK supervised the study, wrote and/or revised the manuscript.

Acknowledgments

The authors thank all participants for their willingness to donate blood, thereby greatly supporting this study. We further thank the Charité Universitätsmedizin Benjamin Franklin Flow Cytometry Core Facility, headed by A. Fernandes and supported by DFG Instrument Grants (INST 335/597-1 FUGG, INST 335/777-1 FUGG). We are grateful for the support of Dr. Nils Lachmann and Dr. Diana Stauch (HLA-lab Charité Universitätsmedizin) for provision of blood from a DPA1*01:03^{+} donor. Graphical illustrations were generated with Biorender.

Funding

AS and KK received funding by the Sonnenfeldstiftung Berlin, Germany. KK was supported by grants from the Deutsche Forschungsgemeinschaft (KO-2270/71, KO-2270/4-1) and unconditional funding from Chiesi GmbH. The funder was not involved in the study design, collection, analysis, interpretation of data, the writing of this article or the decision to submit it for publication. The study was supported by a mentor-based postdoctoral fellowship program in rehabilitation research from the National Multiple Sclerosis Society (MB-1707-28359, to SMG). ES is enrolled in the Charité Clinician Scientist Program funded by the Charité–Universitätsmedizin Berlin and the Berlin Institute of Health. SL is supported by the German Ministry for Education and Research through the Medical Informatics Initiative (junior research group “Medical Omics”, 01ZZ2001).

References

1. Khoury DS, Cromer D, Reynaldi A, Schlub TE, Wheatley AK, Juno JA, et al. Neutralizing antibody levels are highly predictive of immune protection from symptomatic SARS-CoV-2 infection. *Nat Med.* 2021;27(7):1205-11.
2. Ohmit SE, Petrie JG, Cross RT, Johnson E, and Monto AS. Influenza hemagglutination-inhibition antibody titer as a correlate of vaccine-induced protection. *J Infect Dis.* 2011;204(12):1879-85.
3. Almeida JR, Price DA, Papagno L, Arkoub ZA, Sauce D, Bornstein E, et al. Superior control of HIV-1 replication by CD8+ T cells is reflected by their avidity, polyfunctionality, and clonal turnover. *J Exp Med.* 2007;204(10):2473-85.
4. Betts MR, Nason MC, West SM, De Rosa SC, Migueles SA, Abraham J, et al. HIV nonprogressors preferentially maintain highly functional HIV-specific CD8+ T cells. *Blood.* 2006;107(12):4781-9.
5. Sekine T, Perez-Potti A, Rivera-Ballesteros O, Stralin K, Gorin JB, Olsson A, et al. Robust T Cell Immunity in Convalescent Individuals with Asymptomatic or Mild COVID-19. *Cell.* 2020;183(1):158-68 e14.
6. Sattler A, Angermair S, Stockmann H, Heim KM, Khadzhynov D, Treskatsch S, et al. SARS-CoV-2-specific T cell responses and correlations with COVID-19 patient predisposition. *J Clin Invest.* 2020;130(12):6477-89.
7. Bacher P, Rosati E, Esser D, Martini GR, Saggau C, Schiminsky E, et al. Low-Avidity CD4(+) T Cell Responses to SARS-CoV-2 in Unexposed Individuals and Humans with Severe COVID-19. *Immunity.* 2020;53(6):1258-71 e5.
8. Loyal L, Braun J, Henze L, Kruse B, Dingeldey M, Reimer U, et al. Cross-reactive CD4(+) T cells enhance SARS-CoV-2 immune responses upon infection and vaccination. *Science.* 2021;374(6564):eabh1823.
9. San Jose E, Borroto A, Niedergang F, Alcover A, and Alarcon B. Triggering the TCR complex causes the downregulation of nonengaged receptors by a signal transduction-dependent mechanism. *Immunity.* 2000;12(2):161-70.
10. Page G, Sattler A, Kersten S, Thiel A, Radbruch A, and Miossec P. Plasma cell-like morphology of Th1-cytokine-producing cells associated with the loss of CD3 expression. *Am J Pathol.* 2004;164(2):409-17.
11. Huang M, Zhang J, and Chen W. FACS isolation of low percentage human antigen-specific CD8(+) T cells based on activation-induced CD3 and CD8 downregulation. *J Immunol Methods.* 2019;472:35-43.
12. Karsten H, Cords L, Westphal T, Knapp M, Brehm TT, Hermanussen L, et al. High-resolution analysis of individual spike peptide-specific CD4(+) T-cell responses in vaccine recipients and COVID-19 patients. *Clin Transl Immunology.* 2022;11(8):e1410.
13. Low JS, Vaqueirinho D, Mele F, Foglierini M, Jerak J, Perotti M, et al. Clonal analysis of immunodominance and cross-reactivity of the CD4 T cell response to SARS-CoV-2. *Science.* 2021;372(6548):1336-41.
14. Ahl PJ, Hopkins RA, Xiang WW, Au B, Kaliaperumal N, Fairhurst AM, et al. Met-Flow, a strategy for single-cell metabolic analysis highlights dynamic changes in immune subpopulations. *Commun Biol.* 2020;3(1):305.
15. Hartmann FJ, Mrdjen D, McCaffrey E, Glass DR, Greenwald NF, Bharadwaj A, et al. Single-cell metabolic profiling of human cytotoxic T cells. *Nat Biotechnol.* 2021;39(2):186-97.
16. Reischig T, Kacer M, Vlas T, Drenko P, Kielberger L, Machova J, et al. Insufficient response to mRNA SARS-CoV-2 vaccine and high incidence of severe COVID-19 in kidney transplant recipients during pandemic. *Am J Transplant.* 2022;22(3):801-12.
17. Salerno S, Messana JM, Gremel GW, Dahlerus C, Hirth RA, Han P, et al. COVID-19 Risk Factors and Mortality Outcomes Among Medicare Patients Receiving Long-term Dialysis. *JAMA Netw Open.* 2021;4(11):e2135379.

18. Sattler A, Schrezenmeier E, Weber UA, Potekhin A, Bachmann F, Straub-Hohenbleicher H, et al. Impaired humoral and cellular immunity after SARS-CoV-2 BNT162b2 (tozinameran) prime-boost vaccination in kidney transplant recipients. *J Clin Invest.* 2021;131(14).
19. Rincon-Arevalo H, Choi M, Stefanski AL, Halleck F, Weber U, Szelinski F, et al. Impaired humoral immunity to SARS-CoV-2 BNT162b2 vaccine in kidney transplant recipients and dialysis patients. *Sci Immunol.* 2021;6(60).
20. Schrezenmeier E, Bergfeld L, Hillus D, Lippert JD, Weber U, Tober-Lau P, et al. Immunogenicity of COVID-19 Tozinameran Vaccination in Patients on Chronic Dialysis. *Front Immunol.* 2021;12:690698.
21. Stumpf J, Siepmann T, Lindner T, Karger C, Schwobel J, Anders L, et al. Humoral and cellular immunity to SARS-CoV-2 vaccination in renal transplant versus dialysis patients: A prospective, multicenter observational study using mRNA-1273 or BNT162b2 mRNA vaccine. *Lancet Reg Health Eur.* 2021;9:100178.
22. Collier DA, Ferreira I, Kotagiri P, Datir RP, Lim EY, Touizer E, et al. Age-related immune response heterogeneity to SARS-CoV-2 vaccine BNT162b2. *Nature.* 2021;596(7872):417-22.
23. Li M, Yao D, Zeng X, Kasakovski D, Zhang Y, Chen S, et al. Age related human T cell subset evolution and senescence. *Immun Ageing.* 2019;16:24.
24. Jurchott K, Schulz AR, Bozzetti C, Pohlmann D, Stervbo U, Warth S, et al. Highly Predictive Model for a Protective Immune Response to the A(H1N1)pdm2009 Influenza Strain after Seasonal Vaccination. *PLoS One.* 2016;11(3):e0150812.
25. Levine LS, Hiam-Galvez KJ, Marquez DM, Tenvooren I, Madden MZ, Contreras DC, et al. Single-cell analysis by mass cytometry reveals metabolic states of early-activated CD8(+) T cells during the primary immune response. *Immunity.* 2021;54(4):829-44 e5.
26. Ricciardi S, Manfrini N, Alfieri R, Calamita P, Crosti MC, Gallo S, et al. The Translational Machinery of Human CD4(+) T Cells Is Poised for Activation and Controls the Switch from Quiescence to Metabolic Remodeling. *Cell Metab.* 2018;28(6):895-906 e5.
27. Geltink RIK, Kyle RL, and Pearce EL. Unraveling the Complex Interplay Between T Cell Metabolism and Function. *Annu Rev Immunol.* 2018;36:461-88.
28. Stuve P, Minarrieta L, Erdmann H, Arnold-Schrauf C, Swallow M, Guderian M, et al. De Novo Fatty Acid Synthesis During Mycobacterial Infection Is a Prerequisite for the Function of Highly Proliferative T Cells, But Not for Dendritic Cells or Macrophages. *Front Immunol.* 2018;9:495.
29. Mamareli P, Kruse F, Lu CW, Guderian M, Floess S, Rox K, et al. Targeting cellular fatty acid synthesis limits T helper and innate lymphoid cell function during intestinal inflammation and infection. *Mucosal Immunol.* 2021;14(1):164-76.
30. Iwata S, Zhang M, Hao H, Trimova G, Hajime M, Miyazaki Y, et al. Enhanced Fatty Acid Synthesis Leads to Subset Imbalance and IFN-gamma Overproduction in T Helper 1 Cells. *Front Immunol.* 2020;11:593103.
31. Gubser PM, Bantug GR, Razik L, Fischer M, Dimeloe S, Hoenger G, et al. Rapid effector function of memory CD8+ T cells requires an immediate-early glycolytic switch. *Nat Immunol.* 2013;14(10):1064-72.
32. Frauwirth KA, Riley JL, Harris MH, Parry RV, Rathmell JC, Plas DR, et al. The CD28 signaling pathway regulates glucose metabolism. *Immunity.* 2002;16(6):769-77.
33. Chang CH, Curtis JD, Maggi LB, Jr., Faubert B, Villarino AV, O'Sullivan D, et al. Posttranscriptional control of T cell effector function by aerobic glycolysis. *Cell.* 2013;153(6):1239-51.
34. Cham CM, Driessens G, O'Keefe JP, and Gajewski TF. Glucose deprivation inhibits multiple key gene expression events and effector functions in CD8+ T cells. *Eur J Immunol.* 2008;38(9):2438-50.
35. Redeker A, Welten SP, Baert MR, Vloemans SA, Tiemessen MM, Staal FJ, et al. The Quantity of Autocrine IL-2 Governs the Expansion Potential of CD8+ T Cells. *J Immunol.* 2015;195(10):4792-801.

36. Pardi N, Tuyishime S, Muramatsu H, Kariko K, Mui BL, Tam YK, et al. Expression kinetics of nucleoside-modified mRNA delivered in lipid nanoparticles to mice by various routes. *J Control Release.* 2015;217:345-51.
37. Pardi N, Hogan MJ, Naradikian MS, Parkhouse K, Cain DW, Jones L, et al. Nucleoside-modified mRNA vaccines induce potent T follicular helper and germinal center B cell responses. *J Exp Med.* 2018;215(6):1571-88.
38. Brentville VA, Metheringham RL, Gunn B, and Durrant LG. High avidity cytotoxic T lymphocytes can be selected into the memory pool but they are exquisitely sensitive to functional impairment. *PLoS One.* 2012;7(7):e41112.
39. Petrova GV, Naumova EN, and Gorski J. The polyclonal CD8 T cell response to influenza M158-66 generates a fully connected network of cross-reactive clonotypes to structurally related peptides: a paradigm for memory repertoire coverage of novel epitopes or escape mutants. *J Immunol.* 2011;186(11):6390-7.
40. Hatayama Y, Hashimoto Y, and Motokura T. Frequent co-reactivation of Epstein-Barr virus in patients with cytomegalovirus viremia under immunosuppressive therapy and/or chemotherapy. *J Int Med Res.* 2020;48(11):300060520972880.
41. Nicoli F, Clave E, Wanke K, von Braun A, Bondet V, Alanio C, et al. Primary immune responses are negatively impacted by persistent herpesvirus infections in older people: results from an observational study on healthy subjects and a vaccination trial on subjects aged more than 70 years old. *EBioMedicine.* 2022;76:103852.
42. Staras SA, Dollard SC, Radford KW, Flanders WD, Pass RF, and Cannon MJ. Seroprevalence of cytomegalovirus infection in the United States, 1988-1994. *Clin Infect Dis.* 2006;43(9):1143-51.
43. Liu H, Rhodes M, Wiest DL, and Vignali DA. On the dynamics of TCR:CD3 complex cell surface expression and downmodulation. *Immunity.* 2000;13(5):665-75.
44. van der Donk LEH, Ates LS, van der Spek J, Tukker LM, Geijtenbeek TBH, and van Heijst JWJ. Separate signaling events control TCR downregulation and T cell activation in primary human T cells. *Immun Inflamm Dis.* 2021;9(1):223-38.
45. Valitutti S, Muller S, Salio M, and Lanzavecchia A. Degradation of T cell receptor (TCR)-CD3-zeta complexes after antigenic stimulation. *J Exp Med.* 1997;185(10):1859-64.
46. Baniyash M. TCR zeta-chain downregulation: curtailing an excessive inflammatory immune response. *Nat Rev Immunol.* 2004;4(9):675-87.
47. Frentsch M, Arbach O, Kirchhoff D, Moewes B, Worm M, Rothe M, et al. Direct access to CD4+ T cells specific for defined antigens according to CD154 expression. *Nat Med.* 2005;11(10):1118-24.

Figure 1, Sattler et al.

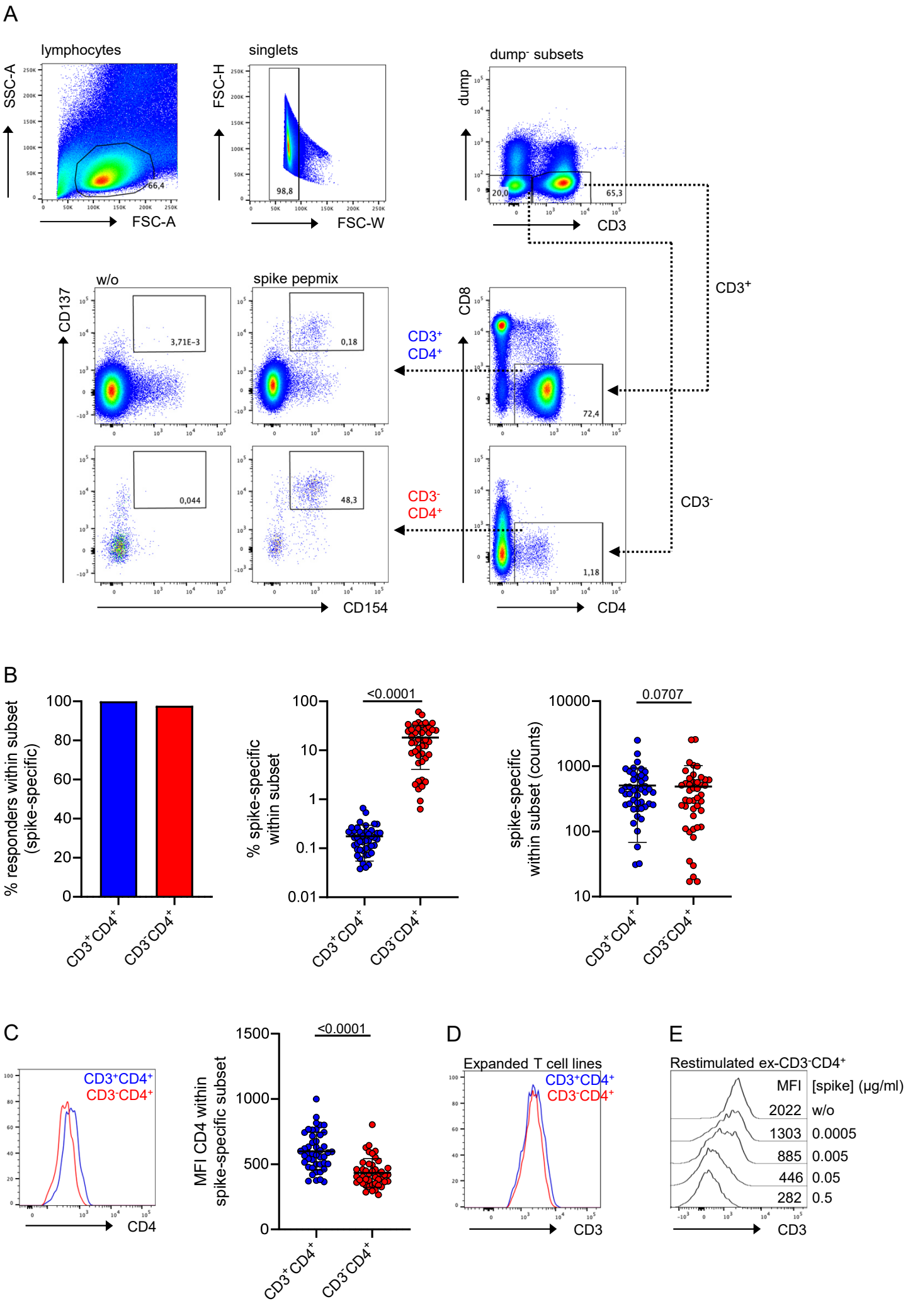

Figure 1

Identification and quantification of vaccine-reactive CD3$^-$CD4$^+$ T helper cells. (A) PBMC were stimulated or not with spike peptide mix for 16 h. Specific CD4$^+$ T helper cells were identified within the CD3$^+$ and CD3$^-$ compartments according to co-expression of CD154 and CD137. (B) Depicts portions of responders (left), frequencies (middle, n=44) and counts (right, n=44) of specific cells in both compartments. (C) Compares CD4 expression levels in the indicated subsets as reflected by mean fluorescence intensity (MFI), n=44. Statistical analyses in A-C were performed using paired, two-tailed Wilcoxon test throughout. Graphs show means ± SD. (D) CD3 expression levels of specific FACS-purified, CD3$^-$CD4$^+$ or CD3$^+$CD4$^+$ -derived T cell lines after 10d of in vitro expansion, representative for n=3. (E) CD3 expression analysis of in vitro expanded, CD3$^-$CD4$^+$ -derived T cell lines after specific restimulation with titrated amounts of antigen; representative for n=3.

Figure 2, Sattler et al.

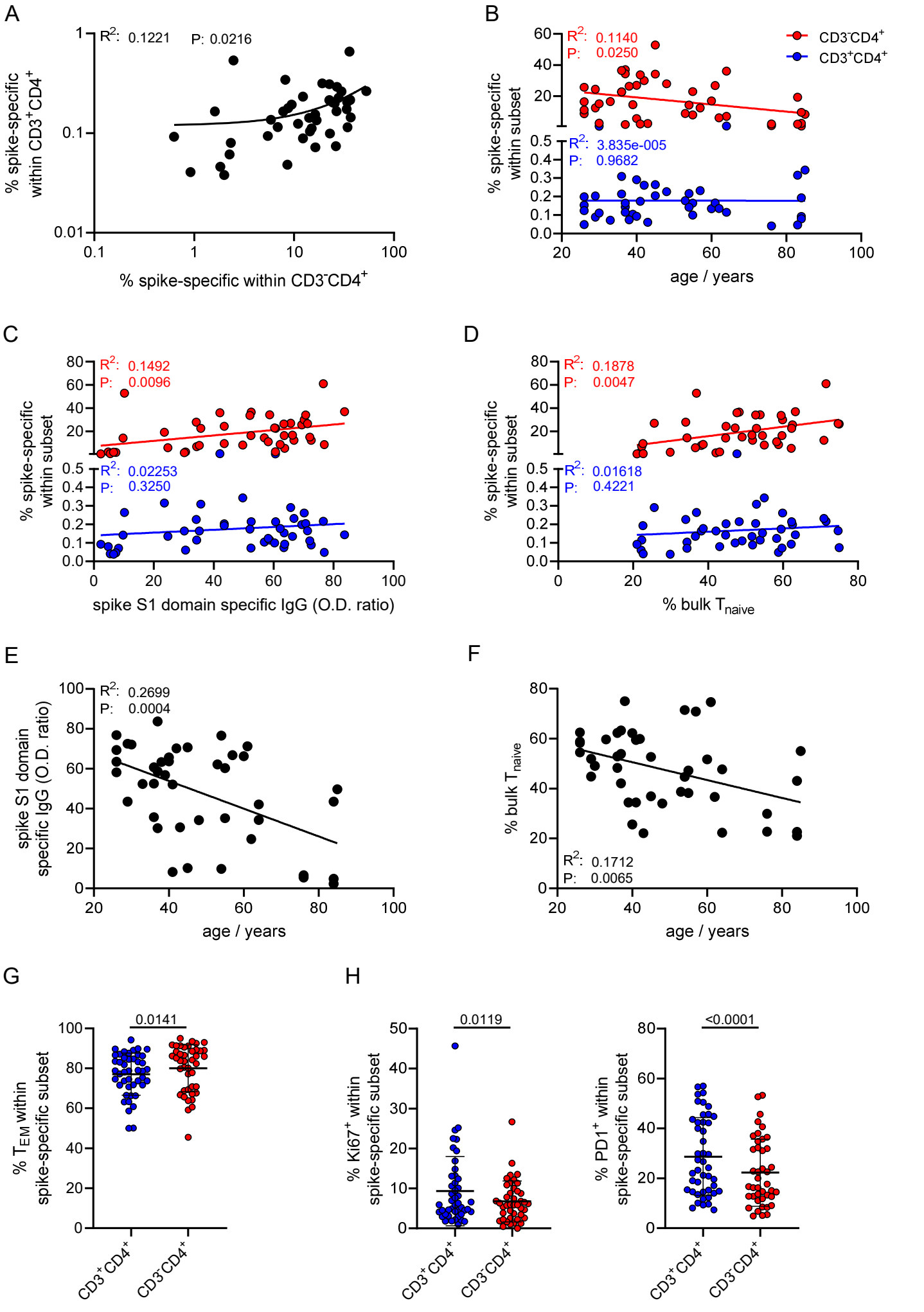

Figure 2

Vaccine-specific CD3$^-$CD4$^+$ Th cells decline with age and positively correlate with specific antibody levels and frequencies of naïve T cells. Frequencies of spike-specific CD3$^-$CD4$^+$ and CD3$^+$CD4$^+$ were determined as before and correlated (A) with each other (n=44), (B) proband age (n=44), (C) spike S1-domain specific IgG levels (n=44), or (D) frequencies of bulk naïve CD45RO$^-$CD62L$^+$ Th cells (n=42). Further analyses address the interrelation of age with specific antibody levels (E) or (F) frequencies of bulk naïve CD45RO$^-$CD62L$^+$ Th cells (both n=42). (G) shows portions of CD45RO$^+$CD62L$^-$ effector/memory-type Th cells in both subsets, whereas (H) quantifies frequencies of spike-specific proliferating Ki67$^+$ (left) or in vivo activated PD1$^+$ (right) Th cells (both n=44); statistical analyses were performed using simple linear regression (A-F) or paired, two-tailed Wilcoxon test (G and H). Where applicable, graphs show means ± SD.

Figure 3, Sattler et al.

A

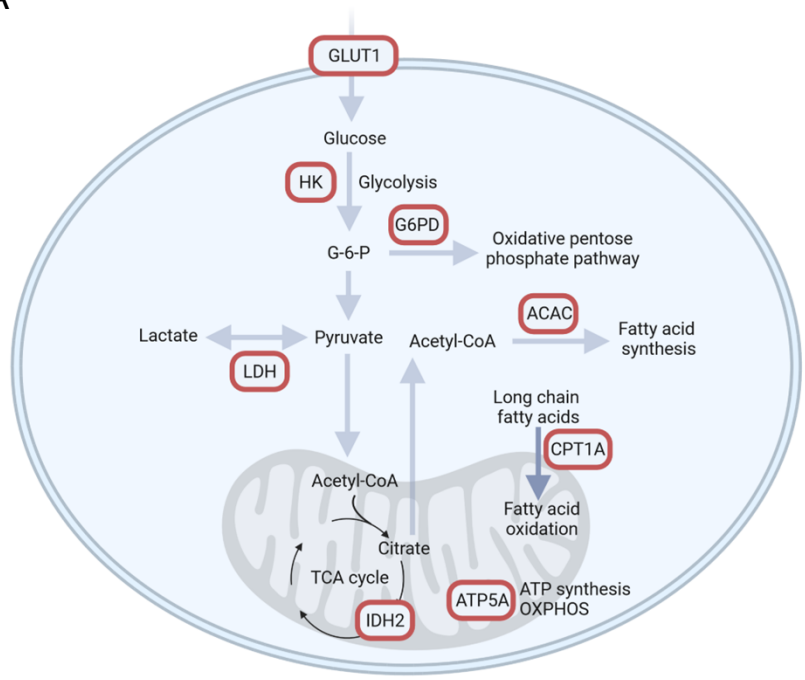

B

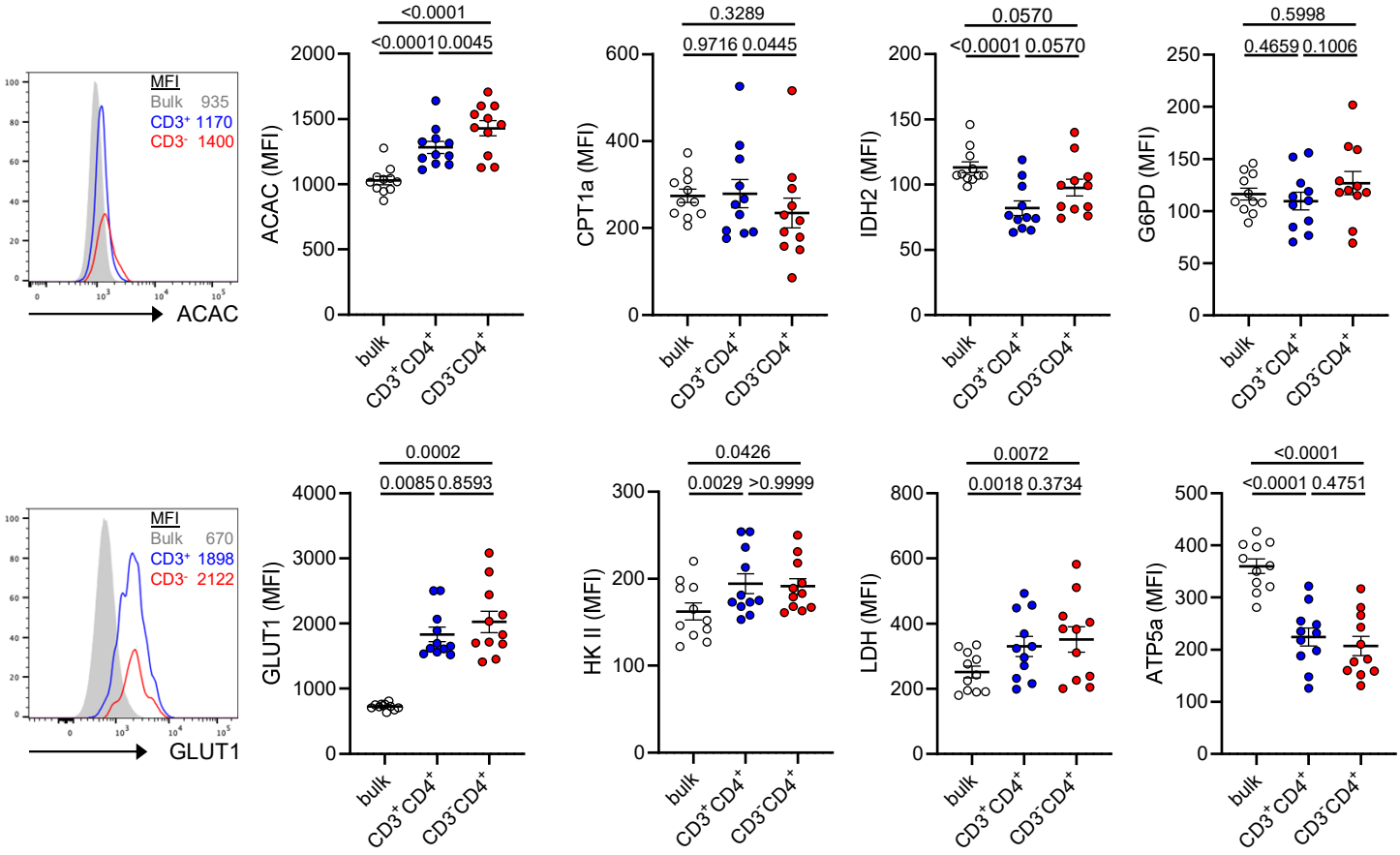

Figure 3

Single-cell metabolic pathway analysis in spike-specific $CD3^{-}CD4^{+}$ T cells. (A) Overview over cell metabolism and key metabolic proteins targeted by flow cytometry. (B) PBMC were stimulated or not with Spike peptide mix for 16 h. The expression level (mean fluorescence intensity) of key metabolic proteins was analyzed in Spike-specific ($CD154^{+}CD137^{+}$) $CD3^{+}CD4^{+}$ vs. $CD3^{-}CD4^{+}$ T cells vs. non-specific $CD154^{-}CD137^{-}CD3^{+}CD4^{+}$ "bulk" control T cells within the same sample. Histograms (upper and lower left) show exemplary expression characteristics in the three subsets for ACAC and GLUT1. n=11; statistical analyses were performed using paired one-way ANOVA (ACAC, CPT1a, G6PD, ATP5a, LDH) or Friedman test (IDH2, GLUT1, HKII). Where applicable, graphs show means ± SD.

Figure 4, Sattler et al.

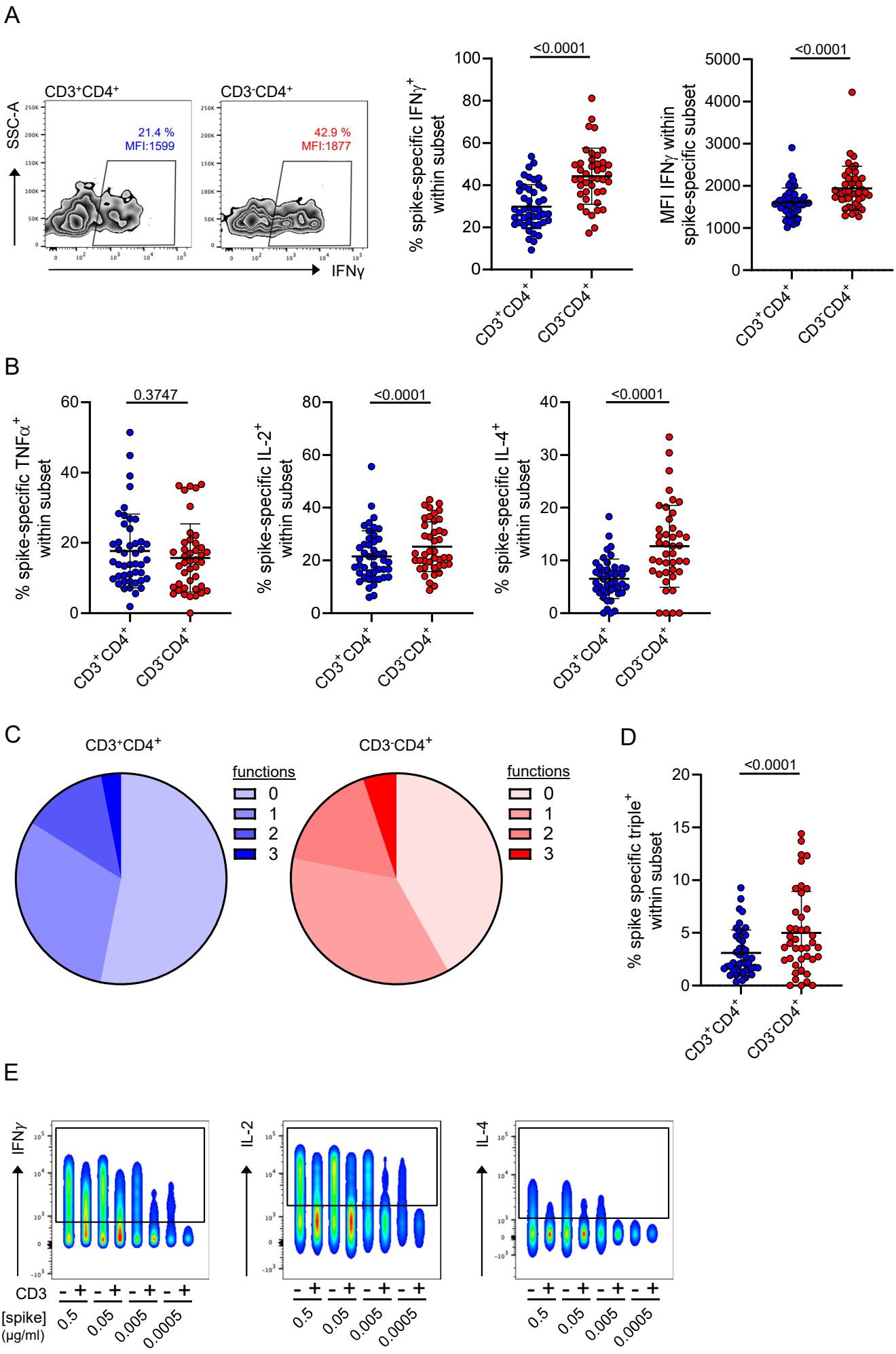

Figure 4

Differential cytokine production capacity by spike-specific $CD3^-CD4^+$ and $CD3^+CD4^+$ Th cell subsets. PBMC were stimulated or not with spike peptide mix for 16 h. Specific $CD4^+$ T helper cells were identified as before and further assessed intracellularly for cytokine production. (A) Exemplary zebra plots (left) and summary of frequencies (middle, n=44) or per-cell expression levels (right, n=44) of $IFN\gamma^+$ T cells within both spike-specific populations. (B) depicts frequencies TNFα (left), IL-2 (middle) or IL-4 (right) expressing spike-specific T cells, all n=44. (C) Mean frequencies of specific cells showing 0, 1, 2 or three functions with respect to IFNγ-, TNFα- and IL-2 expression in both subsets and (D) statistics for $IFN\gamma^+TNF\alpha^+IL\text{-}2^+$ polyfunctional T cells, n=43. Statistical analysis with paired, two-tailed t test (A, left; B, right) or paired, two-tailed Wilcoxon test (all other graphs). Where applicable, graphs show means ± SD. (E) Production of IFNγ, IL-2 and IL-4 in in vitro expanded, FACS-sorted spike-specific $CD3^-CD4^+$ vs. $CD3^+CD4^+$ T cell subsets after restimulation with titrated concentrations of antigen; representative for n=2 donors out of independent experiments.

Figure 5, Sattler et al.

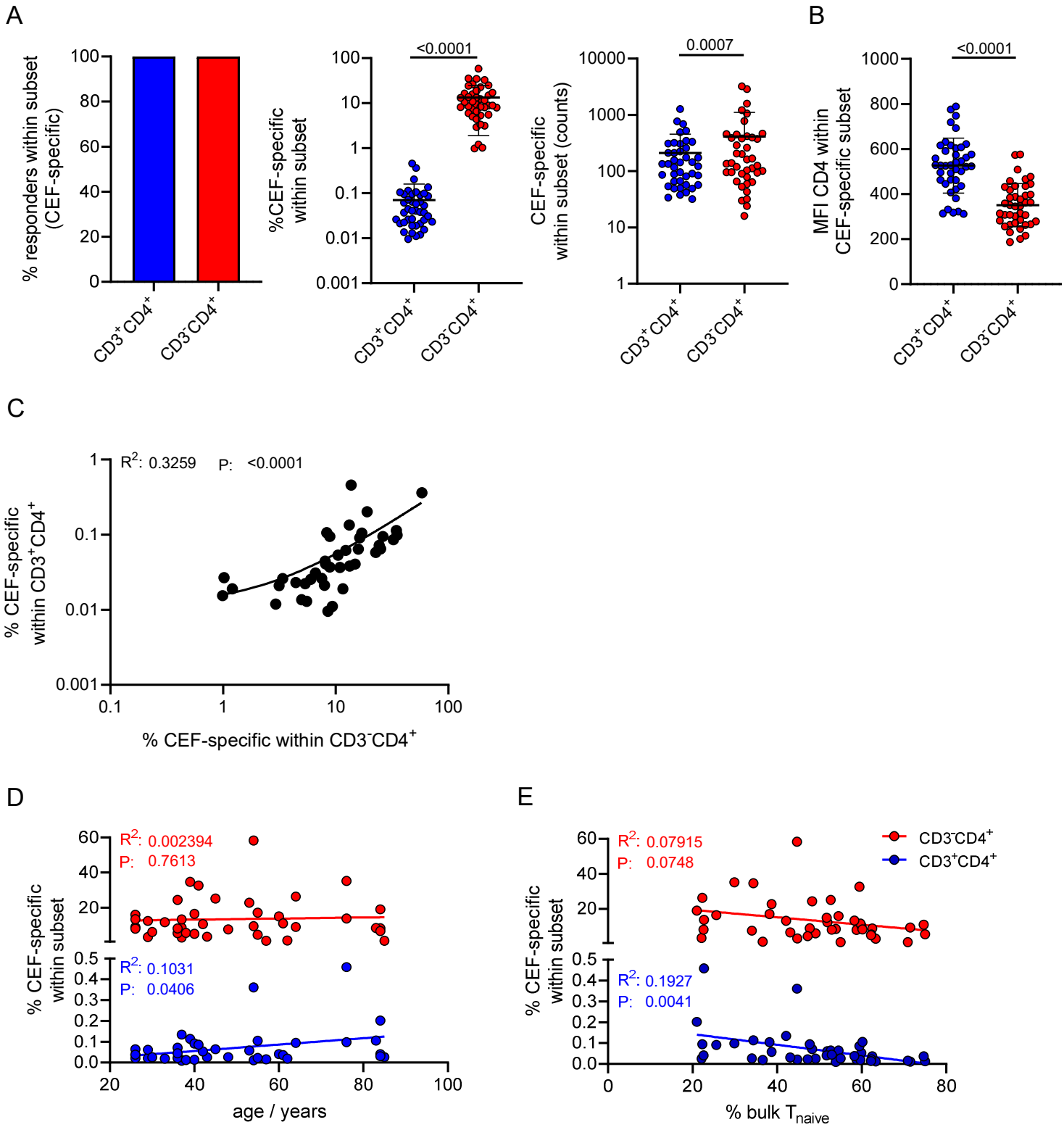

Figure 5

Characterization of the CEF-specific $CD3^-CD4^+$ T cell response. PBMC were stimulated or not with CEF peptide mix for 16 h. Specific $CD4^+$ T helper cells were identified within the $CD3^+$ and $CD3^-$ compartments according to co-expression of CD154 and CD137. (A) Depicts portions of responders (left), and frequencies (middle) and counts (right) of specific cells in both compartments. (B) Displays CD4 expression levels in the indicated subsets as reflected by mean fluorescence intensity. (C) Depicts the correlation between frequencies of both subsets, whereas (D) and (E) show correlations between frequencies and age or the percenteage of bulk naïve $CD45RO^-CD62L^+$ Th cells, respectively. n=41 throughout; statistical analyses were performed using paired, two-tailed Wilcoxon test (A), paired, two-tailed t test (B) or simple linear regression (C-E). Where applicable, graphs show means ± SD.

Figure 6, Sattler et al.

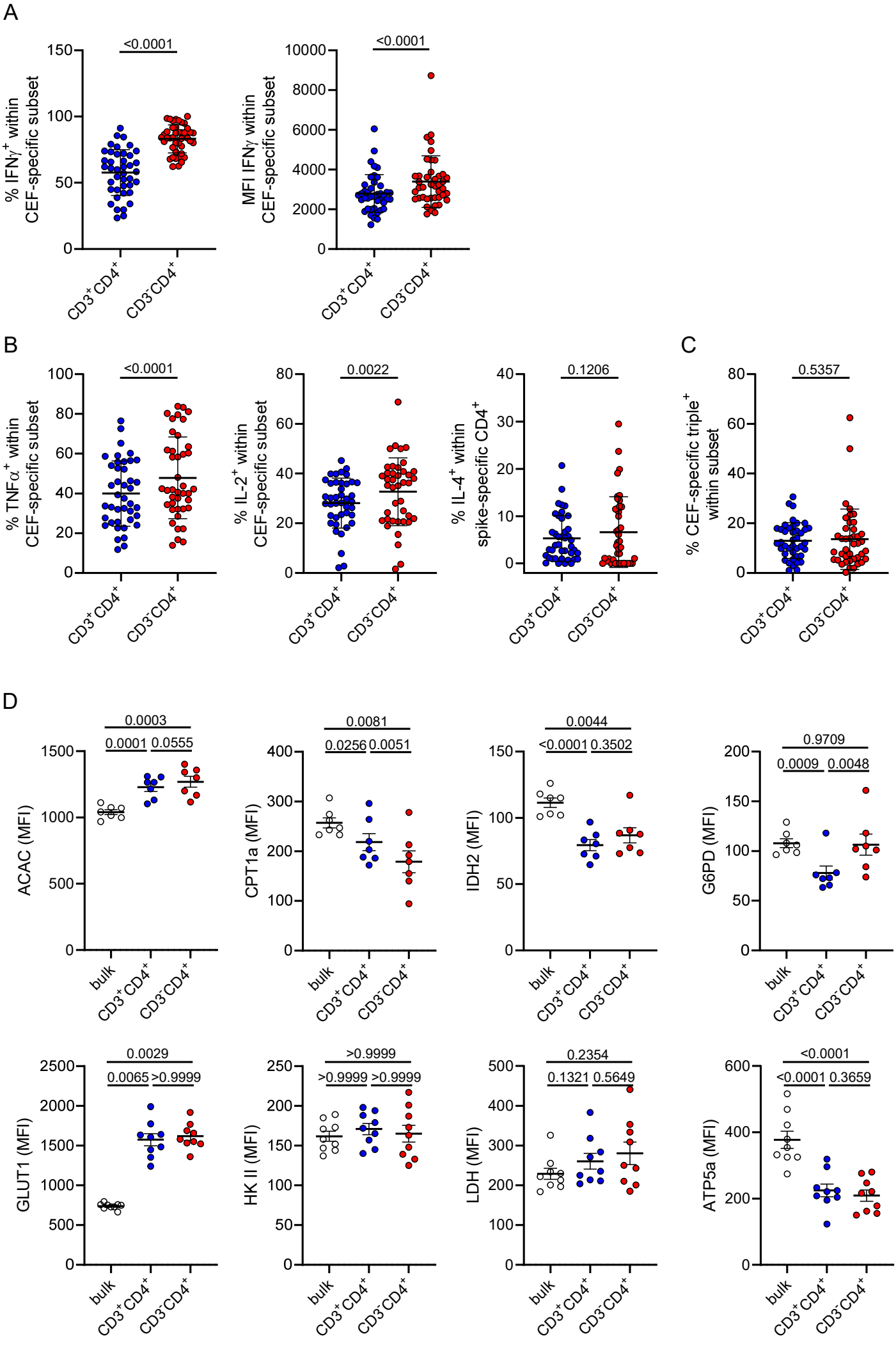

Figure 6

Functional and metabolic assessment of CEF-specific $CD3^-CD4^+$ and $CD3^+CD4^+$ Th cell subsets. PBMC were stimulated or not with CEF peptide mix for 16 h. Specific $CD4^+$ T helper cells were identified as before and further assessed intracellularly for cytokine production. (A) Frequencies (left, n=42) and expression levels (right, n=42) of $IFN\gamma^+$ T cell subsets specific for CEF. (B) Frequencies of TNFα (left), IL-2 (middle) or IL-4 (right) expressing CEF-specific T cells and (C) those of IFNγ-, TNFα- and IL-2 co-expressing polyfunctional T cells. n=41 for all analyses. Statistical analysis with paired, two-tailed t test (A, left, B, middle) or paired, two-tailed Wilcoxon test (remaining graphs). (D) Expression levels (according to mean fluorescence intensity) of the indicated key metabolic proteins were analyzed in CEF-specific ($CD154^+CD137^+$) $CD3^+CD4^+$ vs. $CD3^-CD4^+$ T cells vs. non-specific $CD154^-CD137^-CD3^+CD4^+$ bulk control T cells within the same sample. n=7 (upper panels) and 9 (lower panels); statistical analyses were performed using paired one-way ANOVA (ACAC, CPT1a, IDH2, G6PD, LDH, ATP5a) or Friedman test (GLUT1, HKII). Where applicable, graphs show means ± SD.

Figure 7, Sattler et al.

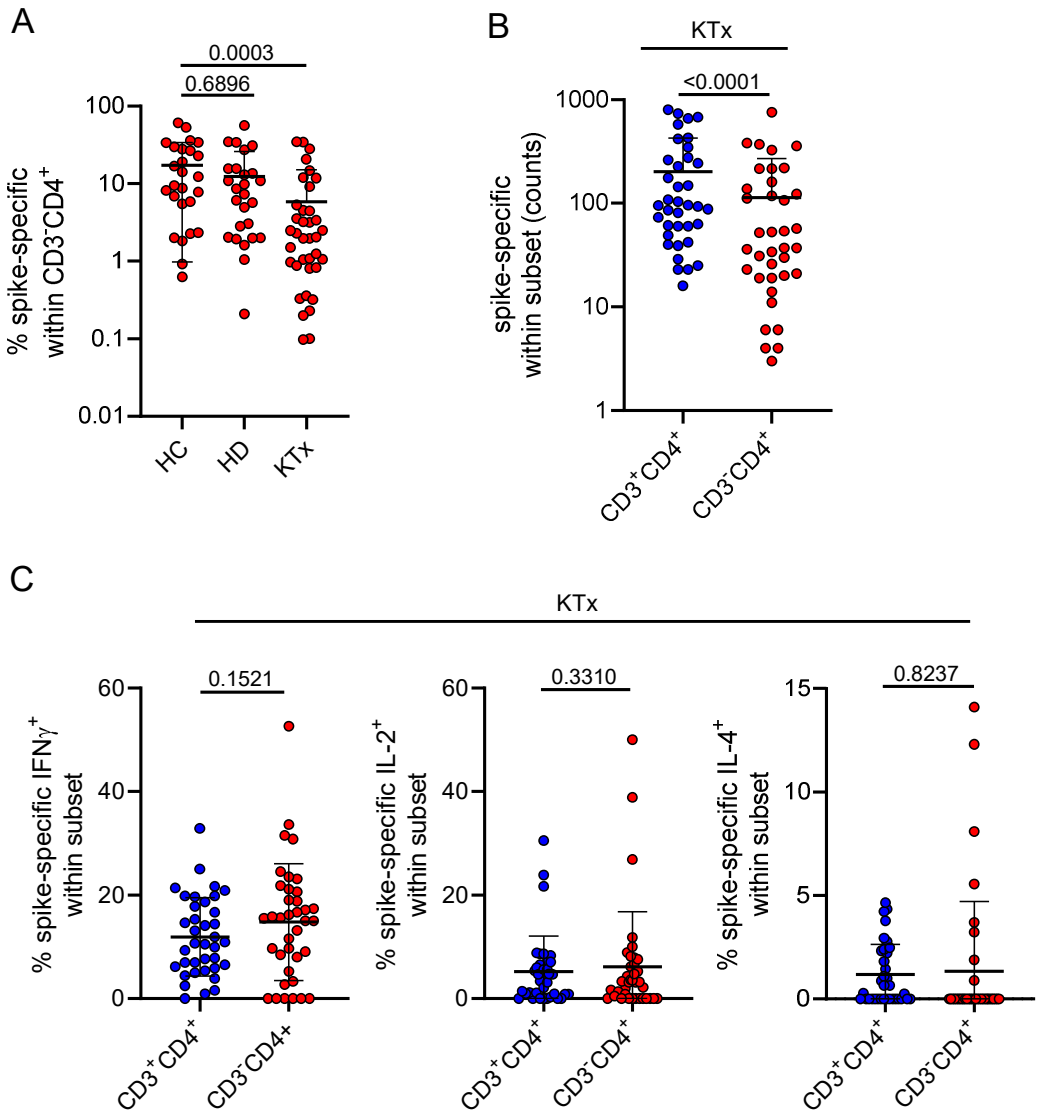

Figure 7

Vaccine-specific CD3$^-$CD4$^+$ Th cells in dialysis patients and kidney transplant recipients. ***(A)*** Spike-specific CD3$^-$CD4$^+$ T cells were identified as before; frequencies were quantified in age-matched healthy controls (HC), patients on hemodialysis (HD) and kidney transplant recipients under immunosuppressive treatment (KTx). Frequencies of (B) spike-specific CD3$^-$ CD4$^+$ and CD3$^+$CD4$^+$ Th cell subsets and (C) portions of IFNγ (left), IL-2 (middle) and IL-4 (right) expressing Th cell subsets in kidney transplant recipients. n=26 (HC)/26 (HD)/37 (KTx). Statistical analysis was performed with Kruskal-Wallis-test (A), paired, two-tailed t test (B, left) or paired, two-tailed Wilcoxon test (all other graphs). Where applicable, graphs show means ± SD.

Table I

Characteristics of healthy probands (n=44) enrolled

Variable	
Age (mean yrs ± SD)	49.75 (18.80)
Females (n, %)	22 (50)
Age males (mean yrs ± SD)	50.82 (18.78)
Age females (mean yrs ± SD)	48.68 (19.21)
Caucasians (n, %)	44 (100)

Table II

Characteristics of healthy probands and patients included, related to data in Figure 7

Variable	HC (n=26)	KTx (n=37)	HD (n=26)	P
Age (mean yrs ± SD)	61.46 (15.56)	58.59 (13.93)	67.19 (11.88)	n.s.
Females (n, %)	12 (46.15)	11 (29.73)	9 (34.62)	n.s.
Caucasians (n, %)	26 (100)	37 (100)	26 (100)	n.s.
Clinical Parameters				
Time on dialysis (mean yrs±SD)			6.87 (5.07)	
Time since Tx (mean yrs±SD)		6.73 (5.26)		
Retransplantation (%)		7 (18.91)		
IS medication				
CS+Tac+MMF (%)		21 (56.76)		
CS+CyA+MMF (%)		13 (35.13)		
$mTOR_i$+MMF±CS (%)		2 (5.41)		
$mTOR_i$+CyA+MMF (%)		1 (2.70)		
Comorbidities				
Hypertension (%)		35 (94.59)	22 (84.61)	
Diabetes (%)		11 (29.73)	12 (46.15)	
Coronary heart disease (%)		7 (18.92)	15 (57.70)	
History of malignancy (%)		5 (13.51)	3 (11.54)	
History of liver disease (%)		4 (10.81)	9 (34.62)	
History of myocardial infarction (%)		3 (8.11)	4 (15.38)	
COPD (%)		0 (0)	3 (11.54)	

CS – Corticosteroids, Tac – Tacrolimus, CyA – Cyclosporin A, MMF – Mycophenolate Mofetil, $mTOR_i$ – mammalian target of rapamycin inhibitor, P – statistical significance, n.s. – not significant